

Efficient Volume Computation for SMT Formulas*

Arijit Shaw

Chennai Mathematical Institute
IAI, TCG-CREST, Kolkata

Uddalok Sarkar

Indian Statistical Institute, Kolkata

Kuldeep S. Meel

Georgia Institute of Technology
University of Toronto

Abstract

Satisfiability Modulo Theory (SMT) has recently emerged as a powerful tool for solving various automated reasoning problems across diverse domains. Unlike traditional satisfiability methods confined to Boolean variables, SMT can reason on real-life variables like bitvectors, integers, and reals. A natural extension in this context is to ask quantitative questions. One such query in the SMT theory of Linear Real Arithmetic (LRA) is computing the volume of the entire satisfiable region defined by SMT formulas. This problem is important in solving different quantitative verification queries in software verification, cyber-physical systems, and neural networks, to mention a few.

We introduce *ttc*, an efficient algorithm that extends the capabilities of SMT solvers to volume computation. Our method decomposes the solution space of SMT Linear Real Arithmetic formulas into a union of overlapping convex polytopes, then computes their volumes and calculates their union. Our algorithm builds on recent developments in streaming-mode set unions, volume computation algorithms, and AllSAT techniques. Experimental evaluations demonstrate significant performance improvements over existing state-of-the-art approaches.

1 Introduction

Satisfiability Modulo Theories (SMT) has revolutionized automated reasoning, serving as the foundational technology for diverse problems [KS16]. The power of SMT stems from its ability to reason over diverse theories, including bitvectors, reals, and integers, extending well beyond the capabilities of traditional SAT solvers [BBB⁺22, BSST21, BB09, CGSS13, NP23]. This versatility has established SMT as the de facto decision procedure not only in formal verification of software and hardware workflows [HJ20, MMB⁺18], but across numerous domains requiring sophisticated logical reasoning, including security [BBB⁺20], test-case generation, synthesis, planning [CMZ20], and optimization [SSA16].

Meanwhile, quantitative reasoning has emerged as a critical advancement in satisfiability solving. Rather than merely determining whether a Boolean formula can be satisfied, model counting [CMV21, GSS21] techniques calculate the number of satisfying assignments — establishing a

*A preliminary version of this work appears at the International Conference on Principles of Knowledge Representation and Reasoning (KR) 2025. The tool *ttc* is available at <https://github.com/meelgroup/ttc>.

robust framework for addressing quantitative challenges like probabilistic inference [CD08], software verification [TW21], network reliability [DOMPV17], neural network verification [BSS⁺19], and numerous other problems [SM24].

The natural evolution of these parallel developments leads to the compelling extension to effectively handle quantitative queries within SMT frameworks. This challenge is nuanced by the diversity of the underlying theories, each demanding different approaches. In discrete domains like bitvectors and linear integer arithmetic, the problem manifests as model counting. For linear real arithmetic, it transforms into volume computation or counting distinct regions. Recent years have witnessed remarkable progress across these domains, yielding both theoretical insights and practical algorithms for bitvectors [CMMV16, CDM15, KM18], linear integers [GB21, Ge24a, GMM⁺19], and strings [ABB15]. But these approaches are mostly limited to discrete domains, and hardly been extended to continuous domains. In this work, we address the question: *Given an SMT LRA formula, can we design an efficient volume computation algorithm?*

Our primary contribution is the development of **ttc**, a novel algorithmic framework that provides an affirmative answer to this question. The **ttc** algorithm approximates the volume of SMT LRA formula solution spaces with provable theoretical guarantees.

We start with a very related and well-studied problem to SMT volume computation: the problem of volume computation of bounded convex bodies. Sophisticated exact and approximate methods to solve the problem have been developed in the last few decades. Although the exact volume problem is $\#P$ -hard, the seminal work by [DFK91] showed a polynomial-time randomized approximation algorithm (FPRAS) for this problem. Furthermore, advancements have not only improved the asymptotic running times of these algorithms [LS90, AK91, Lov91, LS92, LS93, KLS97, LD12, CV18] but also yielded practically efficient methods that forgo certain theoretical guarantees to eliminate prohibitive hidden constants in their runtime [CV16].

A central challenge in applying these ideas to SMT lies in the non-convex nature of the solution spaces generated by SMT formulas. Unlike convex bodies, non-convex regions are more complex to analyze due to their irregular shapes and potential discontinuities. A natural strategy to overcome this hurdle is to partition the non-convex space into a union of convex bodies, where each convex piece can be more easily managed with existing techniques. Decomposing a non-convex SMT solution space into convex components introduces its own set of challenges. Current state-of-the-art techniques can't handle the union of non-disjoint components. In many cases, the decomposition yields an excessive number of disjoint components, which may not accurately reflect the underlying structure of the solution space. In practice, solution spaces manifest as unions of overlapping, non-disjoint polytopical regions with boundaries and intersections that encode critical constraint information. This overlapping structure is not merely theoretical—our empirical analysis reveals cases where state-of-the-art decomposition techniques transform a natural representation of 7 overlapping polytopes into an unwieldy collection of 20,595 disjoint components, creating unnecessary computational complexity.

Our approach builds upon recent advancements in counting distinct elements across set unions in streaming models by [MVC21] (MVC). The fundamental challenge in adapting the MVC algorithm to volume computation arises from the inherent difference between discrete and continuous domains. The MVC algorithm was specifically engineered for discrete settings, while volume computation operates in continuous space. We overcome this obstacle through a principled discretization approach, effectively reducing continuous volume computation to the problem of counting lattice points within a carefully constructed fine-grained lattice space.

We have implemented **ttc** and evaluated it on a comprehensive benchmark suite. The results demonstrate significant gains in scalability and accuracy. Out of a benchmark set of 1131 instances, **ttc** solved 1112, while the current state of the art can solve only 145.

Applications. The theory of linear real arithmetic has significant applications in the formal verification of systems with real variables. These include hybrid systems such as cyber-physical systems [KDM⁺23], and control systems [CMT12] and timed systems [CGSS13]. Advanced verification tools like Reluplex [KBD⁺17] extend SMT solving to neural networks by encoding real-valued variables for network inputs. Extending these approaches to quantitative verification would require LRA solvers with efficient volume computation capabilities. This follows the established pattern where model counting tools have enabled quantitative verification advances in software [GFB21, TW21] and binarized neural networks [BSS⁺19].

2 Notation and Preliminaries

An SMT (Satisfiability Modulo Theories) formula F is a quantifier-free logical formula over a background theory \mathcal{T} that may contain both theory atoms (e.g., linear arithmetic predicates) and pure Boolean variables. We focus on formulas over Linear Real Arithmetic (LRA), where theory atoms are of the form $a_1x_1 + \dots + a_nx_n \circ b$, with $a_i, b \in \mathbb{R}$ and $\circ \in \{<, \leq, =, \geq, >\}$.

The Boolean abstraction F_B of F is obtained by replacing each theory atom with a fresh Boolean variable while leaving the original Boolean variables unchanged. We assume that F_B is expressed in Disjunctive Normal Form (DNF) as $F_B = \bigvee_{i=1}^m c_i$, where each cube is given by $c_i = \bigwedge_{j=1}^{n_i} \ell_{ij}$, with each ℓ_{ij} being a Boolean literal (either a variable or its negation). And-Inverter Graphs (AIGs) are used as a compact representation for Boolean functions as a circuit, where each node corresponds to a two-input AND gate or an inverter.

We define a mapping M on the Boolean literals corresponding to theory atoms such that for each such literal ℓ , $M(\ell)$ is its corresponding linear inequality (or its negation). Pure Boolean variables are not mapped, as they do not contribute geometric constraints. For each cube c_i , the conjunction $\bigwedge_{j=1}^{n_i} M(\ell_{ij})$ (with the understanding that M is applied only to theory literals) defines a (possibly empty) convex polytope, which we denote by $\mathcal{P}(c_i) = \{x \in \mathbb{R}^n \mid \forall \ell \in c_i \text{ (theory literal), } M(\ell)(x) \text{ holds}\}$.

A polyhedron is defined as the intersection of a finite number of half-spaces in \mathbb{R}^n , and a polytope is a bounded polyhedron whose volume (measured via the Lebesgue measure) can be computed. Concretely, any polytope K can be written in the form $\{x \in \mathbb{R}^n \mid Ax \leq b\}$, where A is a $m \times n$ matrix and b is a $n \times 1$ vector. Each row of the system $Ax \leq b$ defines one of the m half-spaces (the facets of K). We denote $\text{facet}(K) = m$, $\text{Sol}(K) = \{x \in \mathbb{R}^n \mid Ax \leq b\}$, and $\text{Volume}(K)$ as the number of facets, the feasible region, and the volume of K , respectively.

```
(set-logic QF_LRA)

(declare-const x Real)
(declare-const y Real)

(assert (or
  (and (> x 20) (< x 40) (> y 20) (< y 40))
  (and (> x 10) (< x 30) (> y 10) (< y 30))))

(check-sat)
```

Figure 1: SMT file.

Illustrative Example. Figure 1 shows the QF_LRA formula over two real variables x and y , which defines two overlapping square regions in the xy -plane. As depicted in Figure 2, each square has an area of 400, with an overlapping area of 100. Thus, the union of the two regions has an area

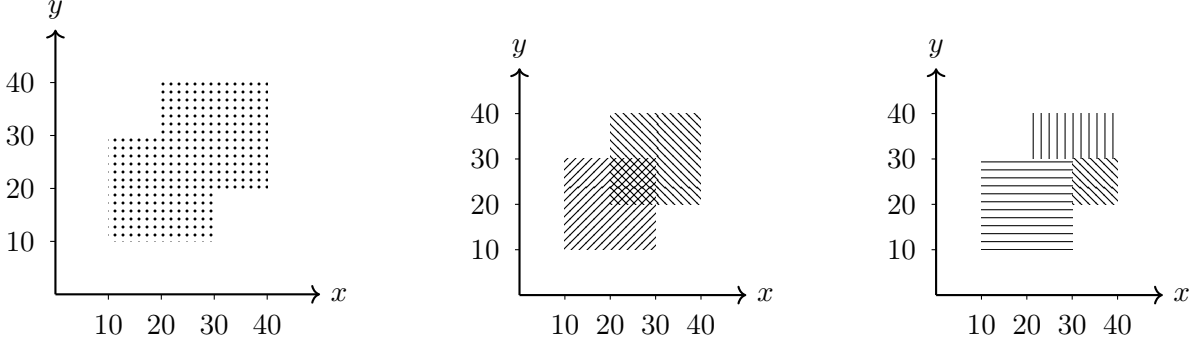


Figure 2: Solution space of SMT formula (left). Disjoint (middle) and non-disjoint (right) decomposition of the solution space of the formula.

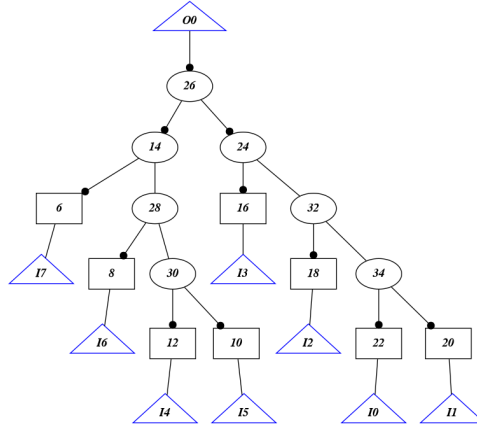


Figure 3: AIG of Boolean abstraction for the example SMT formula, where the variables like 6, 8, 10, 12 correspond to the LRA atoms $x \leq 10, x \geq 30, y \leq 10, y \geq 30$ respectively.

of 700. Figure 3 shows the And-Inverter Graph (AIG) derived from the Boolean abstraction of our linear constraints. Internal nodes represent logical conjunctions, and any inverted edges (dots) indicate negations. Figure 2 (left) illustrates a disjoint decomposition of the solution space, where each region is separated so that no two subsets overlap. This often simplifies volume computations but may require more partitions. By contrast, Figure 2 (right) shows a non-disjoint decomposition, allowing subsets to overlap. Figure 4 compares the number of cubes generated by disjoint decomposition and non-disjoint decomposition on our benchmark set.

Problem Statement Let K be the whole solution space of the given formula F , which has d dimensions. Let $\mathcal{B} \subset \mathbb{R}^n$ be an n -dimensional measurable set. The volume of \mathcal{B} is defined as $V(\mathcal{B}) = \int_{\mathcal{B}} d\mathbf{x}$, where $d\mathbf{x}$ denotes the differential volume element. In Cartesian coordinates, this element is expressed as $d\mathbf{x} = dx_1 dx_2 \cdots dx_n$.

3 Related Work

SMT Volume Computation was first addressed by Ma, Liu, and Zhang, who developed the *vinci* tool [MLZ09] for exact volume computation. Their approach performs intelligent disjoint decomposition of the solution space into convex polytopes using a *bunching* strategy, followed by exact computation of individual polytope volumes. Later, [GMZZ18] designed *polyvest*, which extended *vinci* by incorporating MCMC-based techniques for polytope volume computation. Recently, Ge

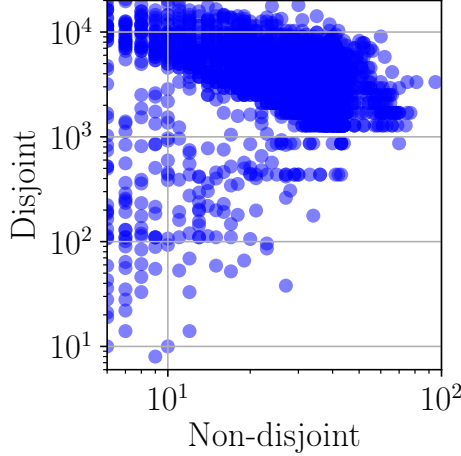


Figure 4: Comparison of the number of polytopes in disjoint and non-disjoint decomposition (notice the non-equal axis).

introduced the **SharpSMT** tool [Ge24b], which integrates and optimizes various techniques from previous work of **polyvest** and **vinci** [GMZZ18, MLZ09] to create a more comprehensive solution for SMT volume computation.

Weighted Model Integration (WMI) [BPVdB15] represents a closely related problem in the hybrid domain of Boolean and rational variables, involving the computation of volume given weight density over the entire domain. This area has seen significant research advances through diverse approaches, including predicate abstraction and All-SMT techniques [MPS17, MPS19], knowledge compilation methods [KMS⁺18], and structurally-aware algorithms [SMM⁺22, SMM⁺24]. However, while WMI focuses primarily on computing weighted integration across domains, our work specifically addresses the fundamental problem of determining the exact volume of the solution space.

Polytope Volume Computation has been a central focus in computational geometry since [DF88] proved it $\#P$ -hard, followed by Dyer, Frieze, and Kannan’s FPRAS development (). Rigorous algorithmic advances have improved complexity bounds from $\tilde{\mathcal{O}}(n^{23})$ to $\tilde{\mathcal{O}}(n^3)$ [AK91, KLS97, LV06, LD12, CV18]¹. Though these algorithms contain large hidden constants, practical implementations have been achieved by carefully relaxing theoretical guarantees [CV16, CF21].

Estimating the size of a set union has been a well-studied problem since the work of Karp and Luby (), who proposed a $\mathcal{O}(m \log^2 |\Omega|)$ -time algorithm, where m denotes the number of sets and $|\Omega|$ represents the universe size. Subsequent research has extensively explored streaming settings, where sets arrive sequentially over time [FM85, GT01, KNW10]. More recent methods employ sampling-based strategies in the context of streaming algorithms [MVC21], which have also been adapted for DNF counting [SSA⁺24]. These approaches achieve a $\tilde{\mathcal{O}}(nm)$ -time complexity for estimating the solution count of a DNF formula, where m is the number of clauses and n is the number of variables in the DNF formula. Our work builds upon and extends techniques developed in the DNF counting framework.

¹ $\tilde{\mathcal{O}}(\cdot)$ hides the polylogarithmic factors in $\mathcal{O}(\cdot)$.

4 Algorithm and Analysis

This section presents the core contribution of our work: the `ttc` algorithm along with its theoretical analysis.

4.1 Algorithm

Given an SMT LRA formula F , the `ttc` algorithm returns an estimate of $\text{Volume}(F)$. Initially, the algorithm decomposes the solution space of the SMT formula into non-disjoint polytopes and computes the volume for each polytope. Subsequently, it estimates the volume of the union of the polytopes' solution space using a sampling-based approach.

Algorithm 1 `ttc`(F, ε, δ)

```

1:  $F_B^A, M \leftarrow \text{BooleanAbstraction}(F)$ 
2:  $C \leftarrow \text{toDNF}(F_B^A)$ 
3:  $b \leftarrow \text{GetPrecision}(C, M, \frac{\varepsilon}{4})$ 
4:  $\varepsilon' \leftarrow \frac{\varepsilon}{12}$ 
5:  $\text{Thresh} \leftarrow \max\left(24 \cdot \frac{\ln(24/\delta)}{(1-\varepsilon')\varepsilon'^2}, 6(\ln \frac{6}{\delta} + \ln m)\right)$ 
6:  $p \leftarrow 1$  ;  $\mathcal{X} \leftarrow \emptyset$ 
7: for  $i = 1$  to  $m$  do
8:    $t \leftarrow \text{Volume}(\text{Polytope}(c_i), \varepsilon', \delta')$ 
9:   for  $s \in \mathcal{X}$  do
10:    if  $s \in \text{Polytope}(c_i)$  then remove  $s$  from  $\mathcal{X}$ 
11:   while  $p \geq \frac{\text{Thresh}}{t}$  do
12:     Remove every element of  $\mathcal{X}$  with prob.  $1/2$ 
13:      $p \leftarrow p/2$ 
14:    $N_i \leftarrow \text{Poisson}(t \cdot p)$ 
15:   while  $N_i + |\mathcal{X}| > \text{Thresh}$  do
16:     Remove every element of  $\mathcal{X}$  with prob.  $1/2$ 
17:      $N_i \leftarrow \text{Poisson}(t \cdot p/2)$  and  $p \leftarrow p/2$ 
18:    $S \leftarrow \text{GenerateSamples}(\text{Polytope}(c_i), N_i, b)$ 
19:    $\mathcal{X}.\text{Append}(S)$ 
20: Output  $|\mathcal{X}|/p$ 

```

Since we only have a volume computation algorithm for convex polytopes, but the solution space of an SMT formula may be non-convex, we decompose the solution space as a union of convex polytopes. First, we observe that using C , the Boolean abstraction of F in DNF form, we can capture the solution space of F as a union of polytopes. Let $c_i = \bigwedge_{j=1}^{n_i} \ell_{ij}$ be a cube in the DNF. Then, the conjunction $\bigwedge_{j=1}^{n_i} M(\ell_{ij})$ of the corresponding linear inequalities defines a (possibly empty) convex polytope, which we denote by $\text{Polytope}(c_i)$. We can show that $\bigcup_{i=1}^m \text{Polytope}(c_i) = \text{Sol}(F)$ ([Lemma 1](#)). This relation shows that the DNF representation of the Boolean abstraction of an SMT formula can be used to decompose its solution space into convex polytopes.

To efficiently compute the union of these polytopes, we leverage recent breakthroughs in streaming algorithms for set union operations. The central idea is to compute the union of volumes by maintaining a representative set of points that approximates the total volume. The main caveat of this approach is that the algorithm requires the underlying sets to be finite, while the volume of a polytope cannot be measured directly with a finite number of points. To

overcome this issue, we consider an axis-parallel lattice in \mathbb{R}^n with cell side length 10^{-b} , defined as $\mathbb{L}^n = 10^{-b}\mathbb{Z}^n = \{(10^{-b}k_1, 10^{-b}k_2, \dots, 10^{-b}k_n) \mid k_i \in \mathbb{Z} \text{ for } i = 1, \dots, n\}$. If b is sufficiently large, we can use this lattice to establish a relationship between the number of lattice points contained within a polytope, $|K \cap \mathbb{L}^n|$, and the volume of the polytope, $\text{Volume}(K)$.

We present our algorithm, `ttc`, in [Algorithm 1](#), and in the subsequent part, we describe the algorithm in detail.

In line 1 of `ttc`, we parse the formula F and construct its Boolean abstraction as a circuit, specifically as an And-Inverter Graph (AIG). Then, in line 2, `ttc` converts the circuit to DNF. The circuit representation enables us to avoid introducing any auxiliary variables. In essence, converting the circuit to DNF is equivalent to solving a circuit AllSAT problem, for which we leverage recent advances in the literature.

Based on the desired accuracy ε of the volume estimate, we begin by computing the precision parameter b using `GetPrecision` in line 3, and threshold value, `Thresh`, in line 5, which determines approximately how many points will be maintained during the algorithm’s execution. In the main loop (lines 7 to 19), we process each cube $\text{Polytope}(c_i)$ sequentially. For each cube, we first compute the (approximate) volume of its corresponding polytope using a polytope volume computation algorithm (line 8). Next, in line 10, the algorithm removes from the current set \mathcal{X} all solutions that are already accounted for. We then determine the number of solutions N_i that would be sampled from $\text{Polytope}(c_i)$ if each solution were independently sampled with probability p ; here, N_i is modeled by a Poisson distribution. Since we wish to keep the size of \mathcal{X} bounded by `Thresh`, if the sum $|\mathcal{X}| + N_i$ exceeds `Thresh`, we decrease p and adjust N_i accordingly—this adjustment is performed by resampling N_i from a Poisson distribution with the revised parameter (p) and by removing elements from \mathcal{X} with probability $1/2$ (line 12). Next, we sample N_i solutions from the cube c_i uniformly at random and add to \mathcal{X} —this is essentially done by uniformly sampling a lattice point from $\text{Polytope}(c_i) \cap \mathbb{L}^n$. Finally, the algorithm outputs the final volume estimate $\frac{|\mathcal{X}|}{p}$.

Getting precision. From [\[KV97\]](#), we know that if an n -dimensional ℓ_2 -ball of radius $\gamma = \Omega(n\sqrt{\log f})$ can be inscribed in an n -dimensional polytope with f facets, then there exists a relationship between the number of integer lattice points inside the polytope and its volume. When working with the lattice \mathbb{L}^n instead of the standard integer lattice \mathbb{Z}^n , the effective radius decreases, but the same relationship still applies. Furthermore, as shown in [Lemma 5](#), the same relationship holds for a union of polytopes, provided each polytope contains an ℓ_2 -ball of radius $\gamma = \Omega(n\sqrt{\log \sum_i \text{facet}(P_i)})$. In [Algorithm 2](#), we process each polytope sequentially (lines 5–9). For each polytope P^i , we compute $\hat{\gamma}$, the maximum radius of a ball that can be inscribed in P^i , using an LP algorithm (line 6). The required precision for this polytope is then determined as $\lceil \log_{10}(\gamma/\hat{\gamma}) \rceil$. After processing all polytopes, we take the maximum of these precision values and return it.

4.2 Analysis

Theorem 1. *Given a set F , and parameters $\varepsilon, \delta \in (0, 1]$, `ttc` returns an estimate $\text{Est of Volume}(F)$ such that with probability at least $1 - \delta$,*

$$\text{Est} \in [(1 - \varepsilon) \cdot \text{Volume}(F), (1 + \varepsilon) \cdot \text{Volume}(F)].$$

We prove the theorem using the following lemmas.

Lemma 1. *Let $C = \bigvee_{i=1}^m c_i$ be the DNF abstraction of the SMT formula F . Then,*

$$\bigcup_{i=1}^m \text{Polytope}(c_i) = \text{Sol}(F)$$

Algorithm 2 GetPrecision(C, M, η)

```
1: maxRatio  $\leftarrow$  1,  $r \leftarrow 0$ 
2: for  $c_i$  in  $C$  do
3:    $P^i \leftarrow \text{Polytope}(c_i)$ 
4:    $r \leftarrow r + \text{facet}(P^i)$ 
5: for  $i = 1$  to  $m$  do
6:    $\hat{\gamma} \leftarrow \text{MaxInscribedBall}(P^i)$ 
7:    $\gamma \leftarrow \frac{16n}{\eta} \sqrt{\log \frac{4r}{\eta}}$ 
8:   if  $\frac{\gamma}{\hat{\gamma}} > \text{maxRatio}$  then
9:     maxRatio  $\leftarrow \frac{\gamma}{\hat{\gamma}}$ 
10: return  $\lceil \log_{10}(\text{maxRatio}) \rceil$ 
```

Proof. First, we show the soundness of each cube: we claim that for every cube c_i in C , $\text{Polytope}(c_i) \subseteq \text{Sol}(F)$. Let $c_i = \bigwedge_{j=1}^{n_i} \ell_{ij}$ be an arbitrary cube of C . By construction, we have $\ell_{i,j} \models C$. Therefore, by the property of Boolean abstraction, if $\bigwedge M(\ell_{i,j})$ can be satisfied, then F is satisfied. Any point $x \in \text{Polytope}(c_i)$ satisfies $\bigwedge M(\ell_{i,j})$, therefore $x \in \text{Sol}(F)$, proving that $\text{Polytope}(c_i) \subseteq \text{Sol}(F)$.

Next, we show the completeness of the union, that $\text{Sol}(F) \subseteq \bigcup_{i=1}^m \text{Polytope}(c_i)$. Consider any arbitrary point $x \in \text{Sol}(F)$. Now x induces a Boolean assignment satisfying C . Since $C = \bigvee_{i=1}^m c_i$, there exists at least one cube c_i such that x satisfies every literal in c_i . By the definition of M , we have that for every $l \in c_i$, $M(l)(x)$ holds, which implies that $x \in \text{Polytope}(c_i)$. Thus, $\text{Sol}(F) \subseteq \bigcup_{i=1}^m \text{Polytope}(c_i)$. \square

We will use the following lemmas in our analysis.

Lemma 2 (Lemma 1 of [SSA⁺24]). *Let N be random variable such that $N \sim \text{Poisson}(\lambda)$, for $\lambda > 0$. Then, for any $x > 0$, the following inequalities hold.*

$$(i) \Pr[|N - \lambda| \geq \zeta] \leq 2 \exp(-\zeta^2/(2\lambda + \zeta))$$

$$(ii) \Pr[N - \lambda \geq \zeta] \leq \exp(-\zeta^2/(2\lambda + \zeta))$$

Lemma 3. *The following three procedures yield statistically equivalent distributions for \mathcal{X} :*

1. *Draw N samples with replacement from a set S , where $N \sim \text{Poisson}(\tilde{s}z \cdot p/2)$ such that $\alpha|S| \leq \tilde{s}z \leq \beta|S|$, where $\beta > \alpha > 0$.*
2. *Draw N samples with replacement from a set S , where $N \sim \text{Poisson}(\tilde{s}z \cdot p)$ such that $\alpha|S| \leq \tilde{s}z \leq \beta|S|$, with $\beta > \alpha > 0$, and then independently discard each sample with probability $1/2$.*
3. *For each point $s \in S$, independently draw $r \sim \text{Poisson}(\tilde{p}/2)$, where $\alpha p \leq \tilde{p} \leq \beta p$, with $\beta > \alpha > 0$, and add r copies of s to \mathcal{X} .*

Proof. Follows from Claim 2 of [SSA⁺24]. \square

Lemma 4 (Theorem 3 of [KV97]). *Let P be a polytope in \mathbb{R}^n that contains an ℓ_2 -ball of radius at least $8n\sqrt{\log(2\text{facet}(P)/\eta)}$, where $0 < \eta \leq 1$ is a constant. Then $\text{Volume}(P)$ satisfies the following bounds,*

$$\text{Volume}(P) \in \left[\frac{1-\eta}{2} |P \cap \mathbb{Z}^n|, (1+\eta) |P \cap \mathbb{Z}^n| \right]$$

We extend this result to the case of the union of polytopes in the following lemma.

Lemma 5. *Let $Q = \bigcup_{i=1}^m P_i$ with $P_i = \text{Polytope}(c_i)$. If every P_i contains an ℓ_2 -ball of radius at least $\frac{16n}{\eta} \sqrt{\log \frac{4r}{\eta}}$ where $0 < \eta \leq 1$ a constant and $r = \sum_{i=1}^m \text{facet}(P_i)$, then*

$$\text{Volume}(Q) \in [(1 - \eta) |Q \cap \mathbb{Z}^n|, (1 + \eta) |Q \cap \mathbb{Z}^n|]$$

Proof. Recall the description of P_i as $P_i = \{x \in \mathbb{R}^n \mid A_{ij}x \leq b_{ij} \ (j = 1, \dots, \text{facet}(P_i))\}$ and set

$$\kappa := \sqrt{2 \log \frac{4}{\eta}} + \sqrt{2 \log r}, \quad k := \max_{i,j} \frac{b_{ij} + \kappa \|A_{ij}\|}{b_{ij} - \kappa \|A_{ij}\|}$$

where $r = \sum_{i=1}^m \text{facet}(P_i)$ and $\|\cdot\|$ denotes the ℓ_2 -norm. Expand/shrink every facet by $\pm \kappa \|A_{ij}\|$ and write $P'_i := \{x \mid A_{ij}x \leq b_{ij} + \kappa \|A_{ij}\|\}$, $P''_i := \{x \mid A_{ij}x \leq b_{ij} - \kappa \|A_{ij}\|\}$, and let $Q' := \bigcup_i P'_i$, $Q'' := \bigcup_i P''_i$. Let X be the randomized rounding process as defined in [KV97], which takes a point $p \in \mathbb{R}^n$ and returns a point in the lattice $x \in \mathbb{Z}^n$ such that $|x - p| \leq 1$. To complete the proof, we will need the following lemma.

Lemma 6. *The following properties hold for the sets Q' and Q'' : (a) Draw p uniformly from the continuous body Q' . Then for every $x \in Q \cap \mathbb{Z}^n$, $\Pr[X_p = x] \geq \frac{1-\eta/2}{\text{Volume}(Q')}$. (b) Draw p uniformly from the continuous body Q'' . The event that p still lies in Q satisfies $\Pr[X_p \in Q] \geq 1 - \frac{\eta}{2}$, and (c) for every $x \in Q \cap \mathbb{Z}^n$, $\Pr[X_p = x] \leq \frac{1}{\text{Volume}(Q'')}$.*

Proof. To begin with the proof we define random variables Y such that We will prove the lemma in two parts. First, we consider that p is drawn uniformly from Q' . Consider the random variable Y such that $Y \in [-1, 1]^n$ that defines the event $X_p = x$ as $x + Y = p$. Then we have,

$$\begin{aligned} \Pr(X_p = x) &= \int_{p \in Q'} \Pr(X_p = x \mid p) \cdot \text{unif}(p) dp \\ &= \int_{p \in Q'} \Pr(X_p = x \mid p) \cdot \frac{dp}{\text{Volume}(Q')} \quad \text{Since unif is uniform over } Q' \\ &= \frac{1}{\text{Volume}(Q')} \int_{p \in Q'} \Pr(x + Y = p) dp \quad \text{since } \Pr(x + Y = p) = \Pr(X_p = x \mid p) \end{aligned}$$

Now since $\Pr(x + Y = p) = 0$ for $p \notin C(x)$ where $C(x)$ is a cube centered at x with all the sides to be of length 1. Therefore,

$$\begin{aligned} \int_{p \in Q'} \Pr(x + Y = p) dp &= \int_{p \in C(x)} \Pr(x + Y = p) dp - \int_{p \in C(x) \setminus Q'} \Pr(x + Y = p) dp \\ &= 1 - \int_{p \in C(x) \setminus Q'} \Pr(x + Y = p) dp \end{aligned}$$

The last equality follows from $\int_{p \in C(x)} \Pr(x + Y = p) dp = 1$, since $Y \in [-1, 1]^n$. Now let us bound $\int_{p \in C(x) \setminus Q'} \Pr(x + Y = p) dp$. Note that, for $x \in Q$, $A_{ij}x \leq b_{ij}$ and $p \in C(x) \setminus Q'$, $A_{ij}p \geq b_{ij} + \kappa \|A_{ij}\|$, therefore $A_{ij}Y \geq \kappa \|A_{ij}\|$. Now for fixed i, j , we consider the random variables $Z_k = \sum_{k'=1}^k A_{ijk'} Y_{k'}$. Since, $\mathbb{E}[Z_k \mid Z_{k-1}] = Z_{k-1}$, we have that Z_k is a martingale. Therefore, since $|Z_k - Z_{k-1}| \leq A_{ijk}$, applying the Azuma's inequality, we have: $\Pr(A_{ij}Y \geq \kappa) \leq 2e^{-\frac{\kappa^2 \|A_{ij}\|^2}{2 \sum_{k'=1}^n |A_{ijk'}|^2}} \leq 2e^{-(\log \frac{4}{\eta} + \log r)} = \frac{\eta}{2r}$. Therefore using union bound, we have:

$$\int_{p \in C(x) \setminus Q'} \Pr(x + Y = p) dp \leq \sum_{ij} \Pr(A_{ij}Y \geq \kappa) \leq \frac{\eta}{2}$$

Therefore,

$$1 - \frac{\eta}{2} \leq \int_{p \in Q'} \Pr(x + Y = p) dp$$

$$\frac{1 - \eta/2}{\text{Volume}(Q')} \leq \Pr(X_p = x)$$

Similarly, if p is sampled from Q'' , we have for every $p \in Q''$,

$$\Pr(X_p \notin Q) \leq \sum_{ij} \Pr(A_{ij}Y \geq \kappa) \leq \frac{\eta}{2}$$

Therefore,

$$\Pr(X_p \in Q) \geq \int_{Q''} \frac{1 - \eta/2}{\text{Volume}(Q'')} dp \geq 1 - \frac{\eta}{2}$$

Again for a fixed $x \in Q \cap \mathbb{Z}^n$, we have:

$$\begin{aligned} \Pr[X_p = x] &= \int_{p \in Q''} \Pr(X_p = x \mid p) \cdot \text{unif}(p) dp \\ &= \int_{p \in Q''} \Pr(X_p = x \mid p) \cdot \frac{dp}{\text{Volume}(Q'')} \quad \text{Since unif is uniform over } Q'' \\ &= \frac{1}{\text{Volume}(Q'')} \int_{p \in Q''} \Pr(x + Y = p) dp \quad \text{since } \Pr(x + Y = p) = \Pr(X_p = x \mid p) \\ &\leq \frac{1}{\text{Volume}(Q'')} \int_{p \in C(x)} \Pr(x + Y = p) dp \quad \text{since in } Q'' \setminus C(x) \text{ else the probability is 0} \\ &= \frac{1}{\text{Volume}(Q'')} \end{aligned}$$

□

We now use this lemma to complete the proof. Consider the case where p is drawn uniformly from Q'' . Then using [lemma 6\(b\)](#) and [6\(c\)](#) we have:

$$\begin{aligned} 1 - \frac{\eta}{2} &\leq \sum_{x \in Q \cap \mathbb{Z}^n} \Pr[X_p = x] \\ &\leq \sum_{x \in Q \cap \mathbb{Z}^n} \frac{1}{\text{Volume}(Q'')} \leq \frac{|Q \cap \mathbb{Z}^n|}{\text{Volume}(Q)} \end{aligned}$$

The last inequality follows from $Q \subseteq Q''$. Since for all $0 < \eta \leq 1$ we have, $(1 - \frac{\eta}{2})^{-1} \leq (1 + \eta)$, therefore, $\text{Volume}(Q) \leq (1 + \eta)|Q \cap \mathbb{Z}^n|$. Again, consider the case where p is drawn uniformly from Q' . Then, using [lemma 6\(a\)](#)

$$\begin{aligned} 1 &\geq \sum_{x \in Q \cap \mathbb{Z}^n} \Pr[X_p = x] \\ &\geq \sum_{x \in Q \cap \mathbb{Z}^n} \frac{1 - \eta/2}{\text{Volume}(Q')} = \left(1 - \frac{\eta}{2}\right) \cdot \frac{|Q \cap \mathbb{Z}^n|}{\text{Volume}(Q')} \end{aligned}$$

Now consider $p \in Q'$. Then $A_{ij}p \leq b'_{ij}$ for all i, j and therefore $A_{ij}\frac{p}{k} \leq b''_{ij}$ for all i, j . This implies that $\frac{p}{k} \in Q''$. This implies that $Q' \subseteq kQ''$. Therefore, $\text{Volume}(Q') \leq k^n \text{Volume}(Q'')$.

Since each P_i contains an ℓ_2 -ball of radius at least $\frac{16n}{\eta} \sqrt{\log \frac{4r}{\eta}}$, it follows that for the pair i, j at which k is attained, we have $b_{ij} \geq \frac{16n}{\eta} \sqrt{\log \frac{4r}{\eta}} \|A_{ij}\|$. Consequently,

$$k^n = \left(\frac{\frac{16n}{\eta} \sqrt{\log \frac{4r}{\eta}} + \kappa}{\frac{16n}{\eta} \sqrt{\log \frac{4r}{\eta}} - \kappa} \right)^n$$

Claim 1. For $n \in \mathbb{N}$ we have,

$$k^n \leq \frac{1 + \eta/4}{1 - \eta/4}$$

Using Claim 1, we can upper bound $\text{Volume}(Q')$ as follows: $\text{Volume}(Q') \leq \frac{1+\eta/4}{1-\eta/4} \cdot \text{Volume}(Q'') \leq \frac{1+\eta/4}{1-\eta/4} \cdot \text{Volume}(Q)$. Using the inequality $\frac{1-\eta/4}{1+\eta/4} \cdot (1 - \frac{\eta}{2}) \geq (1 - \eta)$ for all $0 < \eta \leq 1$, we have $\text{Volume}(Q) \geq (1 - \eta)|Q \cap \mathbb{Z}^n|$, completing the proof of the lemma. \square

Lemma 7. Let $Q = \bigcup_{i=1}^m P_i$ with $P_i = \text{Polytope}(c_i)$ such that every P_i follows the condition of lemma 5, then we have the following bound on the number of lattice points in Q ,

$$\text{Volume}(Q) \in \left[\frac{1 - \eta}{10^{b \cdot n}} |Q \cap \mathbb{L}^n|, \frac{1 + \eta}{10^{b \cdot n}} |Q \cap \mathbb{L}^n| \right]$$

where b is the precision parameter selected by `GetPrecision`.

Proof. We define a canonical isomorphism $\phi : \mathbb{L}^n \rightarrow \mathbb{Z}^n$. For convenience, we use the same notation to denote the image of a polytope P_i (resp. Q) under ϕ , writing $\phi(P_i)$ (resp. $\phi(Q)$). This mapping scales the distance between any two consecutive points $[a, b]$ along a dimension by 10^b . Consequently, a ball of radius r in \mathbb{L}^n corresponds to a ball of radius $10^b r$ in \mathbb{Z}^n . Furthermore, the volume of a polytope P_i (resp. Q) scales by a factor of $10^{b \cdot n}$ when transformed into \mathbb{Z}^n , leading to $\text{Volume}(P_i) \cdot 10^{b \cdot n}$ (resp. $\text{Volume}(Q) \cdot 10^{b \cdot n}$). Since the mapping ϕ preserves the lattice structure, we have $|\phi(P_i) \cap \mathbb{Z}^n| = |P_i \cap \mathbb{L}^n|$ and $|\phi(Q) \cap \mathbb{Z}^n| = |Q \cap \mathbb{L}^n|$.

Finally, the choice of b as selected by `GetPrecision` guarantees that each P_i contains a ball of radius at least $10^{-b} \frac{16n}{\eta} \sqrt{\log(4 \sum_{i=1}^m \text{facet}(P_i)/\eta)}$. Therefore, we can apply lemma 5 to complete the proof. \square

Lemma 8. *numlattice* Let $Q = \bigcup_{i=1}^m \text{Polytope}(c_i)$. Then `ttc` outputs an estimate `Est` such that with probability at least $1 - \delta$,

$$\text{Est} \in \left[\frac{(1 - \varepsilon/4)}{10^{b \cdot n}} |Q \cap \mathbb{L}^n|, \frac{(1 + \varepsilon/4)}{10^{b \cdot n}} |Q \cap \mathbb{L}^n| \right]$$

Proof. Let $\varepsilon' = \frac{\varepsilon}{12}$ as defined in line 4. We denote the polytope corresponding to c_i as $P^i = \text{Polytope}(c_i)$. Let $S^{(i)}$ represent the set of lattice points within all polytopes up to index i , that is, $S^{(i)} = \bigcup_{j \leq i} (P^j \cap \mathbb{L}^n)$. We also define, $\mathcal{X}_j^{(i)}$ as the state of \mathcal{X} after consuming P^i when the value of p is $\frac{1}{2^j}$. Before proceeding with the proof, we introduce the following key invariant:

Invariant For any $i \in [m]$ and $j \geq 0$ the multiset $\mathcal{X}_j^{(i)}$ contains k copies of each lattice point inside $S^{(i)}$, where k is a random variable drawn from $\text{Poisson}(\tilde{p}_j)$ such that $\frac{(1 - \varepsilon')}{2^j 10^{b \cdot n}} \leq \tilde{p}_j \leq \frac{(1 + \varepsilon')}{2^j 10^{b \cdot n}}$.

Lemma 7 ensures that for any P^i , $\text{Volume}(P^i) \in \left[\frac{(1-\varepsilon')}{10^{b \cdot n}} |P \cap \mathbb{L}^n|, \frac{(1+\varepsilon')}{10^{b \cdot n}} |P \cap \mathbb{L}^n| \right]$. Therefore, the invariant follows from **lemma 3**. Now let us define two events corresponding to the run of the algorithm:

1. E_j^{noise} : After consuming the last polytope P^m , the value of p is $\frac{1}{2^j}$.
2. E_j^{error} : At the end of the algorithm $\mathcal{X}_j^{(m)} \notin [(1-\varepsilon')\tilde{p}_j |P \cap \mathbb{L}^n|, (1+\varepsilon')\tilde{p}_j |P \cap \mathbb{L}^n|]$.

Noting that $(1-\varepsilon')\tilde{p}_j \geq \frac{(1-\varepsilon/4)}{2^j 10^{b \cdot n}}$ and $(1+\varepsilon')\tilde{p}_j \leq \frac{(1+\varepsilon/4)}{2^j 10^{b \cdot n}}$ for all $\varepsilon > 0$, it suffices to establish the following bound is enough to complete the proof of the lemma:

$$\Pr \left[\bigcup_{j=0}^{\infty} (E_j^{\text{noise}} \wedge E_j^{\text{error}}) \right] \leq \delta.$$

Let j^* be the smallest j such that $\frac{1}{2^j 10^{b \cdot n}} < \frac{\text{Thresh}}{4|S^{(m)}|}$. Applying union bound, we get

$$\Pr \left[\bigcup_{j=0}^{\infty} (E_j^{\text{noise}} \wedge E_j^{\text{error}}) \right] \leq \sum_{j=0}^{j^*-1} \Pr [E_j^{\text{error}}] + \Pr [\cup_{j \geq j^*} E_j^{\text{noise}}]$$

We now bound these terms separately.

Bounding $\Pr [\cup_{j \geq j^*} E_j^{\text{noise}}]$: For $j < j^*$, we have $\frac{1}{2^j 10^{b \cdot n}} \geq \frac{\text{Thresh}}{4|S^{(m)}|}$. Since the invariant ensures that $\mathcal{X}_j^{(m)}$ contains k copies of each lattice point in $S^{(m)}$, where $k \sim \text{Poisson}(\tilde{p}_j)$, Therefore, by **lemma 3**, we have that $\mathcal{X}_j^{(m)}$ follows $\text{Poisson}(|S^{(m)}|\tilde{p}_j)$ distribution. The event $\cup_{j \geq j^*} E_j^{\text{noise}}$ occurs if p decreases from $\frac{1}{2^{j^*-1}}$ to $\frac{1}{2^{j^*}}$ for some $i \leq m$. This is equivalent to the case that $\mathcal{X} > \text{Thresh}$ for some $\mathcal{X} \sim \text{Poisson}(\frac{|S^{(i)}|}{2^{j^*-1} 10^{b \cdot n}})$. Since from the choice of j^* we have, $\text{Thresh} > \frac{4|S^{(m)}|}{2^{j^*} 10^{b \cdot n}}$, therefore $\text{Thresh} - \frac{|S^{(i)}|}{2^{j^*-1} 10^{b \cdot n}} > \frac{\text{Thresh}}{2}$. Thus, $\Pr[\mathcal{X} > \text{Thresh}]$ can be bounded as follows:

$$\Pr \left[\mathcal{X} - \frac{|S^{(i)}|}{2^{j^*-1} 10^{b \cdot n}} > \text{Thresh} - \frac{|S^{(i)}|}{2^{j^*-1} 10^{b \cdot n}} \right] \leq \Pr \left[\mathcal{X} - \frac{|S^{(i)}|}{2^{j^*-1} 10^{b \cdot n}} > \frac{\text{Thresh}}{2} \right]$$

Applying **lemma 2**, for any $i \leq m$ we have, $\Pr[\mathcal{X} > \text{Thresh}] \leq \exp(-\frac{\text{Thresh}}{6}) \leq \frac{\delta}{6m}$. The last inequality follows from $\text{Thresh} \geq 6 \log(6m/\delta)$. Therefore, by union bound over $i \in [m]$, $\Pr [\cup_{j \geq j^*} E_j^{\text{noise}}] \leq \frac{\delta}{6}$.

Bounding $\sum_{j=0}^{j^*-1} \Pr [E_j^{\text{error}}]$: By noting that $\mathcal{X}_j^{(m)}$ follows $\text{Poisson}(|S^{(m)}|\tilde{p}_j)$ distribution, therefore using **lemma 2** we have that for any $j < j^*$,

$$\Pr [E_j^{\text{error}}] \leq 2 \exp \left(-\frac{\varepsilon'^2 |S^{(m)}| \tilde{p}_j}{3} \right)$$

Now from the definition of j^* we have $\frac{|S^{(m)}|}{2^{j^*-1} 10^{b \cdot n}} > \frac{\text{Thresh}}{4}$, hence $|S^{(m)}|\tilde{p}_{j^*-1} > \frac{(1-\varepsilon')\text{Thresh}}{8}$. Consequently,

$$\Pr [E_j^{\text{error}}] \leq 2 \exp \left(-\frac{\varepsilon'^2 |S^{(m)}| \tilde{p}_{j^*-1}}{3} \right) \leq 2 \exp \left(-\frac{(1-\varepsilon')\varepsilon'^2 \text{Thresh}}{24} \right)$$

Therefore, we have that,

$$\begin{aligned} \sum_{j=0}^{j^*-1} \Pr [\mathbf{E}_j^{\text{error}}] &\leq 2 \exp \left(-\frac{(1-\varepsilon')\varepsilon'^2 \text{Thresh}}{24} \right) + 2 \exp \left(-\frac{(1-\varepsilon')\varepsilon'^2 \text{Thresh}}{12} \right) + \dots \\ &\leq 4 \exp \left(-\frac{(1-\varepsilon')\varepsilon'^2 \text{Thresh}}{24} \right) \leq \frac{\delta}{6} \end{aligned}$$

The last inequality follows from $\text{Thresh} \geq \frac{24 \log(24/\delta)}{(1-\varepsilon')\varepsilon'^2}$. \square

Proof of theorem 1. Using lemma 8, we have $\text{Est} \geq \frac{1-\varepsilon/4}{10^{b \cdot n}} \cdot |Q \cap \mathbb{L}^n|$, and from lemma 7, $\frac{|Q \cap \mathbb{L}^n|}{10^{b \cdot n}} \geq \frac{\text{Volume}(Q)}{(1+\varepsilon/4)}$. Combining these two inequalities, we get $\text{Est} \geq \frac{1-\varepsilon/4}{1+\varepsilon/4} \cdot \text{Volume}(Q) \geq (1-\varepsilon) \cdot \text{Volume}(Q)$. Similarly, the corresponding upper bounds from lemma 8 and lemma 7 we yield $\text{Est} \leq \frac{1+\varepsilon/4}{1-\varepsilon/4} \cdot \text{Volume}(Q) \leq (1+\varepsilon) \cdot \text{Volume}(Q)$. \square

Theorem 2. *The ttc algorithm takes exponential time w.r.t. v in decomposing the polytope, where v is the number of variables in F_B^A . The number of cubes m can be exponential of v as well.*

Proof. The runtime complexity follows from the dual-rail algorithm of circuit AllSAT algorithm. There exists CNF formulas, for which DNF representation is exponential sized, resulting in the exponential blowup of m . \square

Theorem 3. *Let m denote the number of decomposed polytopes. Then the ttc algorithm runs in time $\mathcal{O}(mn^4)$, where n is the number of dimensions and the $\mathcal{O}(\cdot)$ notation suppresses polylogarithmic factors in ε and δ .*

Proof. The algorithm's main loop (lines 7–19) executes exactly m iterations. In each iteration, the volume computation (line 8) requires $\mathcal{O}(n^4)$ time, while the sampling step (line 18) consumes $\mathcal{O}(n^3)$ time per sample. Since these two operations dominate the computational cost in each iteration, the total runtime is given by $m \times \mathcal{O}(n^4) = \mathcal{O}(mn^4)$, where the polylogarithmic dependencies on ε and δ are hidden in the $\mathcal{O}(\cdot)$ notation. \square

4.3 Implementation

We implemented a Python prototype for testing the algorithm and its efficiency. We use the following tools for different parts of the Algorithm 1.

Decomposing into Polytopes. We use a combination of the existing SMT solver and Circuit AllSAT solver to decompose the SMT solution space into convex polytopes. Specifically, we do the following:

Boolean Abstraction. To create the Boolean abstraction of the SMT formula in line 1 of Algorithm 1, we instrument CVC5 [BBB⁺22] to create the abstraction as an AIG. By default, CVC5 creates the abstraction as a CNF, which we wanted to avoid, since converting to CNF introduces numerous auxiliary variables, making it difficult to enumerate the solutions in a DNF form. For this purpose, we carefully examined each different type of Boolean operation used in SMT formulas, which is typically translated to CNF, including And, Or, Iff, Implies, Ite, and Xor. For each of these operations, we constructed corresponding gates for the AIG. This avoids unnecessary blow-up and retains the semantic structure of the original formula.

Circuit to DNF. To convert the AIG to DNF in line 2, we use the HALL tool [FNS23, FNSS24], which employs a dual-rail based implementation to generate all solutions of the AIG. The solutions are represented as a non-disjoint DNF.

Constructing the Polytopes. While instrumenting CVC5 to generate the Boolean abstraction, we simultaneously capture which variables correspond to which linear inequalities. For each *cube* of the DNF, therefore, we maintain a mapping indicating which set of linear inequalities this cube corresponds to. Given this map and the cube, we construct the polytope.

Polytope Volume Computation. For volume computation in line 8, we employ the Gaussian cooling-based algorithm developed by [CV16], which offers a more practical implementation of their theoretically rigorous approach [CV18]. While the original algorithm [CV18] provides volume approximation with (ε, δ) guarantees, its prohibitive running time of $10^{16}\mathcal{O}(n^3)$ limits practical applications. The key insight in [CV16] was that these substantial constant factors can be significantly reduced in practical scenarios without severely compromising accuracy, though this comes at the cost of theoretical guarantees. Our implementation utilizes VolEsti, the software package by Chalkis and Fisikopoulos () that implements this practical algorithm.

Preprocessing The polytopes generated by the Polytope(c) procedure may contain redundancies and hidden equalities. Hidden equalities render the polytope *degenerate* - resulting in zero volume in d dimensions. Additionally, redundancies significantly complicate the volume computation for the underlying algorithm. We address these challenges by incorporating CDD as a preprocessing step, which effectively identifies hidden equalities and eliminates redundant inequalities. This preprocessing phase yields substantial performance improvements, particularly valuable when processing inequalities derived from SMT files, which often lack optimal formulation.

Polytope Sampling. For polytope sampling, we employ the Monte Carlo random walk hit-and-run algorithm [Smi84]. Each random walk begins from a point within the convex body and executes a specified number of steps, termed the *walk length*. Greater walk lengths produce final points less correlated with the starting position. The number of steps required to generate an uncorrelated point, one approximately sampled from a distribution, is known as the *mixing time*. Lovász and Vempala () showed that $10^{10}\mathcal{O}(n^2)$ is a sufficient mixing time for hit and run. However, such requirements are computationally intractable in practice. Following the empirical observations of Lovász and Deák (), we therefore constrain our implementation to n steps of hit-and-run, which offers a reasonable balance between sampling quality and computational efficiency.

Compromises. While `ttc` is theoretically sound, the implementation involves a few compromises that prioritize efficiency over strict adherence to theoretical guarantees:

1. For volume approximation, algorithms with theoretical guarantees require a running length of $10^{16}\mathcal{O}(n^3)$ steps, which is impractical. Therefore, in our implementation (line 8), we use a practical volume algorithm that employs a convergence-based criterion to determine running length.
2. The sampling algorithm in line 18 relies on the hit-and-run method. Known results indicate that achieving independent samples requires $10^{10}n^2$ steps, which is also impractical. However, Lovász and Deák () demonstrated that taking n steps of hit-and-run provides practically independent samples. As a result, we use n steps in our implementation.

It is worth noting that the state-of-the-art tool, **SharpSMT** (in the non-exact mode i.e., when relying on `polyvest`), also makes similar compromises, and therefore, `ttc` and **SharpSMT** (in non-exact mode) have similar behavior. The exact mode of **SharpSMT**, on the other hand, fails to scale to larger instances, as demonstrated in the following section.

5 Experimental Evaluation

We evaluated our implementation concerning both efficiency and accuracy.

Baseline. For performance evaluation, we used the current state of the art volume computation framework **SharpSMT**², which offers two distinct modes: the **polyvest** algorithm, which estimates the volume, and **vinci**, which performs exact volume computation. To establish meaningful comparisons, we utilized **polyvest** for performance analysis and **vinci** for accuracy check.

Benchmarks. As a first step, we sought to rely on benchmarks from SMT-Lib, but these benchmarks could not be handled by **polyvest** or **vinci** owing to them containing extremely thin geometric regions where dimensions may be constrained to narrow ranges (e.g., $(0, 10^{-7})$). In these cases, **polyvest** and **vinci** fail to handle the required precision and incorrectly classify these polytopes as degenerate with zero volume. Such a study would simply showcase the ability of **ttc** to handle constraints requiring high precision arithmetic but would not allow a more meaningful comparison with **SharpSMT**. Accordingly, we focus on the construction of synthetic instances that are disjunctions of intersecting polytopes, with each polytope defined in H-representation ($Ax \leq b$). In total, our benchmark suite consists of 1131 benchmarks.

1. We vary two parameters: (1) dimension parameter n : ranges from 6 to 34, (2) number of polytopes m : ranges from 6 to 42.
2. For each instance, we generate polytopes using three different geometric shapes studied by [CV16]: (a) *Cubes*: n -dimensional cubes with random bounds, then translated and rotated. (b) *Zonotypes*: Minkowski sum of n different d -dimensional vectors generated randomly. (c) *Simplex*: Shapes where all coordinates are nonnegative and sum to at most 1, defined as $\{x \in \mathbb{R}^n : \sum_{i=1}^n x_i \leq 1, x_i \geq 0\}$.

Environment. We conducted all our experiments on a high-performance computer cluster, with each node consisting of Intel Xeon Gold 6148 CPUs. We allocated one CPU core and a 5GB memory limit to each solver instance pair. To adhere to the standard timeout used in model counting competitions, we set the timeout for all experiments to 3600 seconds. We use values of $\varepsilon = 0.8$ and $\delta = 0.2$, in line with prior work in the model counting community.

With the above setup, we conduct extensive experiments to understand the following:

- RQ1.** How does the runtime performance of **ttc** compare to that of **polyvest**?
- RQ2.** How does the performance of **ttc** scale with different benchmark parameters?
- RQ3.** How accurate is the count computed by **ttc** in comparison to the exact count?

Summary of Results. **ttc** achieves a significant performance improvement over **polyvest** by finishing on 1112 instances in a benchmark set consisting of 1131, while **polyvest** could only finish on 145 instances. **polyvest** barely finishes on instances with more than 25 polytopes or 20 dimensions, while **ttc** seamlessly handles 40 polytopes of 35 dimensions. The accuracy of the approximate count is also noteworthy, with an average error of a count by **ttc** of only 0.059.

5.1 Performance of **ttc**

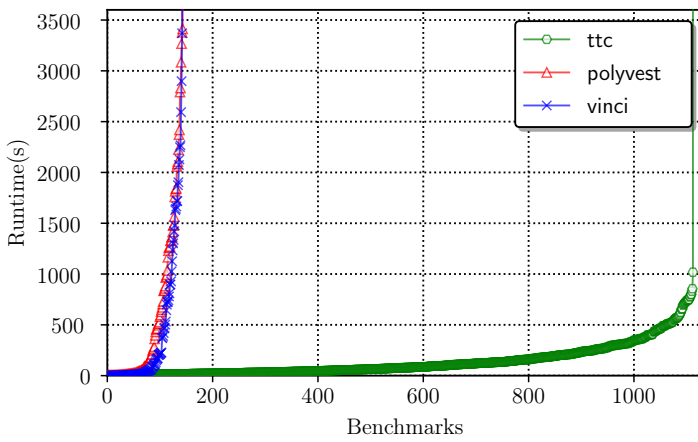
Instances Solved. In **Table 1**, we compare the number of benchmarks that can be solved by **polyvest** and **ttc**. First, it is evident that the **polyvest** only solved 145 out of the 1131 benchmarks in the test suite, indicating its lack of scalability. Conversely, **ttc** solved 1112 instances, demonstrating a substantial improvement compared to **polyvest**.

²Available at <https://github.com/bearben/sharpsmt>

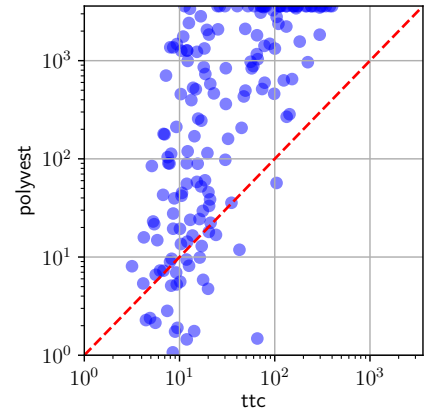
Solver	Solved	PAR-2
vinci	142	6097.63
polyvest	145	6199.73
ttc	1112	255.48

Table 1: Performance comparison on 1131 instances.

Solving Time Comparison. A performance evaluation of **polyvest** and **ttc** is depicted in **Figure 5a**, which is a cactus plot comparing the solving time. The x -axis represents the number of instances, while the y -axis shows the time taken. A point (i, j) in the plot represents that a solver solved j benchmarks out of the 1131 benchmarks in the test suite in less than or equal to j seconds. The curves for **polyvest** and **ttc** indicate that for a few instances, **polyvest** was able to give a quick answer, while in the long run, **ttc** could solve many more instances given any fixed timeout.



(a) Cactus plot comparing runtime of different tools.



(b) Runtime comparison of **ttc** w.r.t. **polyvest**.

Figure 5: Performance comparison: (a) cactus plot of runtimes, (b) scatter plot comparing **ttc** and **polyvest**.

In **Table 1** we also show the PAR-2 score of the solvers, which is the mean runtime over all instances, assigning a cost of $2T$ to each instance timed out at T . **ttc** shows significantly small PAR-2 score. In **Figure 5b**, we present a comparative analysis of solving times between **ttc** and **polyvest**. Each data point (x, y) represents an instance that was solved in x seconds by **ttc** and y seconds by **polyvest**. Points appearing below the dotted red diagonal line indicate instances where **polyvest** outperformed **ttc** in solving time. **ttc** demonstrates superior performance on the vast majority of instances.

5.2 Scaling

In **Figure 6a** and **6b**, we evaluate the scalability of **ttc** and **polyvest** with respect to both the number of polytopes and dimensions. The plots are organized with the number of polytopes increasing from left to right along the x -axis, while the number of dimensions increases from top to bottom along the y -axis. Each pixel corresponds to a specific instance in our benchmark dataset, with the color intensity representing the solver's runtime performance. As demonstrated in **Figure 6a**, **polyvest** exhibits significant performance degradation when handling instances exceeding 12 polytopes or 12 dimensions. By contrast, **Figure 6b** reveals that **ttc** efficiently processes configurations with up to 40 polytopes and 35 dimensions without notable performance

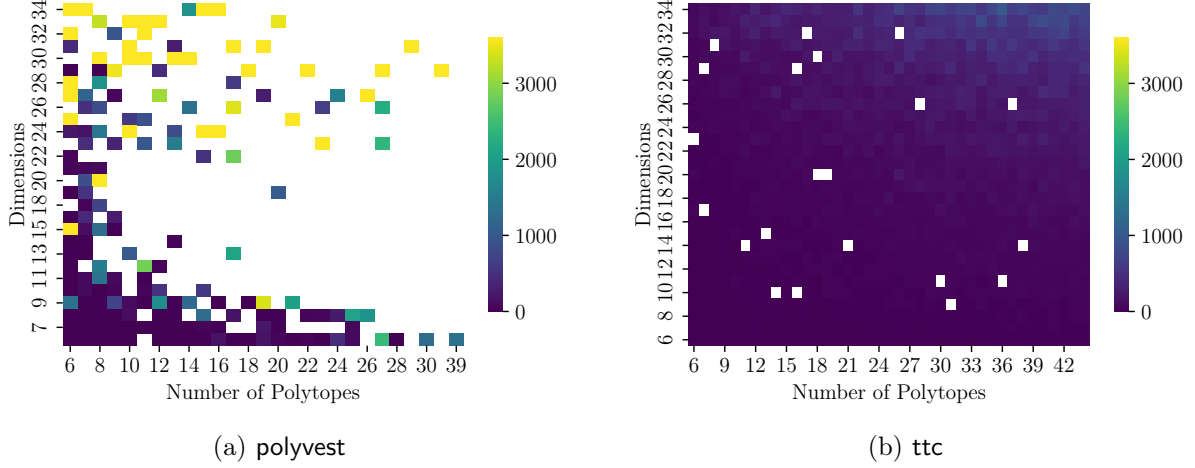


Figure 6: Time taken by w.r.t. dimensions and number of polytopes for **ttc** and **polyvest**.

deterioration. These results clearly establish **ttc** as a substantially more robust and reliable solution for high-dimensional problems involving numerous polytopes.

5.3 Quality of Approximation

In our experimental evaluation, we found the exact volume of 142 benchmarks from **vinci**, enabling us to calculate the error made by **ttc** on these instances. We quantify the error made by **ttc** by the parameter $e = \frac{|b-s|}{b}$, where b represents the count from **vinci** and s from **ttc**. This measure is the *observed error*, analogous to the theoretical error guarantees provided by **ttc**. Analysis of all 142 cases found the median e to be 0.059, geometric mean 0.038, and maximum 0.39, contrasting sharply with a theoretical guarantee of 0.8. This signifies **ttc** substantially outperforms its theoretical bounds. In [Figure 7](#) we plot the observed error, where x -axis, we have the benchmarks, and on the y -axis we have the observed errors. The observed error is below 0.2 for most of the instances.

In [Table 3](#) we showed different observed errors when we run **ttc** with different ϵ values. The median and maximum observed errors decrease with the theoretical ϵ . The maximum *observed error* with $\epsilon = 0.1$, is greater than theoretical, which is not unnatural, given the (ϵ, δ) guarantee nature.

Experiment with different ϵ . [Table 2](#) reports the runtime of **ttc** for varying values of ϵ . The runtime remains largely consistent across different settings. Notably, with $\epsilon = 0.1$, **ttc** solves only two fewer instances compared to $\epsilon = 0.8$, indicating that **ttc** maintains its efficiency even at lower values of ϵ .

Solver	Solved	PAR-2
vinci	142	6097.63
polyvest	145	6199.73
ttc-0.1	1110	275.52
ttc-0.4	1113	248.04
ttc-0.8	1112	255.48

Table 2: Instances solved with different ϵ for **ttc**.

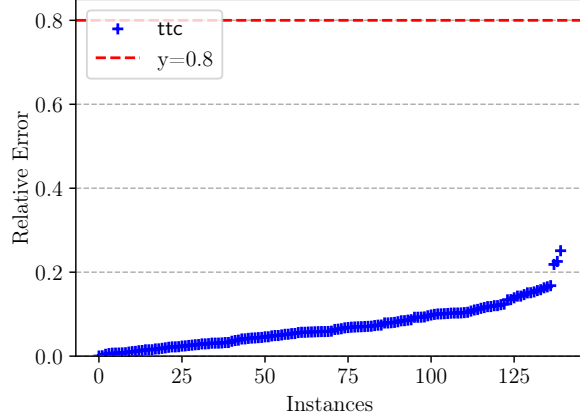


Figure 7: Quality of approximation: observed error on different instances. Sorted according to the observed error.

Theoretical		0.1	0.4	0.8
Observed	Median	0.03	0.04	0.04
	Max	0.22	0.20	0.39

Table 3: Theoretical vs. observed error at different ε .

6 Conclusion

This paper introduces **ttc**, a scalable approximate SMT volume computation tool that demonstrates exceptional performance on practical benchmarks. Our approach harnesses probabilistic techniques to deliver theoretical guarantees on computation results, and empirical results significantly surpassing theoretical guarantees. Our work suggests several promising research directions. First, many formulas contain equality constraints that result in zero volume when computing in d dimensions. A natural extension would be to develop methods for correctly computing $(d - k)$ -dimensional volume in such cases. Second, while we prioritized performance over strict theoretical guarantees in our implementation, experimental results consistently demonstrate error rates well below theoretical bounds. This raises the intriguing question, whether rigorous guarantees can be established for our current implementation without sacrificing its performance advantages.

References

- [ABB15] Abdalbaki Aydin, Lucas Bang, and Tevfik Bultan. Automata-based model counting for string constraints. In *Proc. of CAV*, 2015.
- [AK91] David Applegate and Ravi Kannan. Sampling and integration of near log-concave functions. In *Proceedings of the twenty-third annual ACM symposium on Theory of computing*, pages 156–163, 1991.
- [BB09] Robert Brummayer and Armin Biere. Boolector: An efficient SMT solver for bit-vectors and arrays. In *Proc. of TACAS*, 2009.
- [BBB⁺20] John Backes, Ulises Berrueco, Tyler Bray, Daniel Brim, Byron Cook, Andrew Gacek, Ranjit Jhala, Kasper Luckow, Sean McLaughlin, Madhav Menon, et al. Stratified abstraction of access control policies. In *Proc. of CAV*, 2020.
- [BBB⁺22] Haniel Barbosa, Clark Barrett, Martin Brain, Gereon Kremer, Hanna Lachnitt, Makai Mann, Abdalrhman Mohamed, Mudathir Mohamed, Aina Niemetz, Andres Nötzli, et al. cvc5: A versatile and industrial-strength smt solver. In *Proc. of TACAS*, 2022.
- [BPVdB15] Vaishak Belle, Andrea Passerini, and Guy Van den Broeck. Probabilistic inference in hybrid domains by weighted model integration. In *Proc. of IJCAI*, 2015.
- [BSS⁺19] Teodora Baluta, Shiqi Shen, Shweta Shinde, Kuldeep S Meel, and Prateek Saxena. Quantitative verification of neural networks and its security applications. In *Proc. of CCS*, 2019.
- [BSST21] Clark Barrett, Roberto Sebastiani, Sanjit A Seshia, and Cesare Tinelli. Satisfiability modulo theories. In *Handbook of satisfiability*. 2021.
- [CD08] Mark Chavira and Adnan Darwiche. On probabilistic inference by weighted model counting. *Artificial Intelligence*, 2008.
- [CDM15] Dmitry Chistikov, Rayna Dimitrova, and Rupak Majumdar. Approximate counting in SMT and value estimation for probabilistic programs. In *Proc. of TACAS*, 2015.
- [CF21] Apostolos Chalkis and Vissarion Fisikopoulos. volesti: Volume approximation and sampling for convex polytopes in \mathbb{R} . *R Journal*, 13(2), 2021.
- [CGSS13] Alessandro Cimatti, Alberto Griggio, Bastiaan Joost Schaafsma, and Roberto Sebastiani. The mathsat5 SMT solver. In *Proc. of TACAS*, 2013.
- [CMMV16] Supratik Chakraborty, Kuldeep Meel, Rakesh Mistry, and Moshe Vardi. Approximate probabilistic inference via word-level counting. In *Proc. of AAAI*, 2016.
- [CMT12] Alessandro Cimatti, Sergio Mover, and Stefano Tonetta. Smt-based verification of hybrid systems. In *Proceedings of the AAAI Conference on Artificial Intelligence*, volume 26, pages 2100–2105, 2012.
- [CMV21] Supratik Chakraborty, Kuldeep S Meel, and Moshe Y Vardi. Approximate model counting. In *Handbook of Satisfiability*. 2021.
- [CMZ20] Michael Cashmore, Daniele Magazzeni, and Parisa Zehtabi. Planning for hybrid systems via satisfiability modulo theories. *Journal of Artificial Intelligence Research*, 2020.

- [CV16] Ben Cousins and Santosh Vempala. A practical volume algorithm. *Mathematical Programming Computation*, (2), 2016.
- [CV18] Ben Cousins and Santosh Vempala. Gaussian cooling and $o^*(n^3)$ algorithms for volume and gaussian volume. *SIAM Journal on Computing*, 47(3):1237–1273, 2018.
- [DF88] M. E. Dyer and A. M. Frieze. On the complexity of computing the volume of a polyhedron. *SIAM Journal on Computing*, 17(5):967–974, 1988.
- [DFK91] Martin Dyer, Alan Frieze, and Ravi Kannan. A random polynomial-time algorithm for approximating the volume of convex bodies. *Journal of the ACM (JACM)*, 38(1):1–17, 1991.
- [DOMPV17] Leonardo Duenas-Osorio, Kuldeep Meel, Roger Paredes, and Moshe Vardi. Counting-based reliability estimation for power-transmission grids. In *Proc. of AAAI*, 2017.
- [FM85] Philippe Flajolet and G Nigel Martin. Probabilistic counting algorithms for data base applications. *Journal of computer and system sciences*, 31(2):182–209, 1985.
- [FNS23] Dror Fried, Alexander Nadel, and Yogev Shalmon. Allsat for combinational circuits. In *Proc. of SAT*, 2023.
- [FNSS24] Dror Fried, Alexander Nadel, Roberto Sebastiani, and Yogev Shalmon. Entailing generalization boosts enumeration. In *27th International Conference on Theory and Applications of Satisfiability Testing (SAT 2024)*, pages 13–1. Schloss Dagstuhl–Leibniz-Zentrum für Informatik, 2024.
- [GB21] Cunjing Ge and Armin Biere. Decomposition strategies to count integer solutions over linear constraints. In *Proc. of IJCAI*, 2021.
- [Ge24a] Cunjing Ge. Approximate integer solution counts over linear arithmetic constraints. In *Proc. of AAAI*, 2024.
- [Ge24b] Cunjing Ge. sharpsmt: A scalable toolkit for measuring solution spaces of smt(la) formulas. *Frontiers of Computer Science (FCS)*, 2024.
- [GFB21] Guillaume Girol, Benjamin Farinier, and Sébastien Bardin. Not all bugs are created equal, but robust reachability can tell the difference. In *International Conference on Computer Aided Verification*. Springer, 2021.
- [GMM⁺19] Cunjing Ge, Feifei Ma, Xutong Ma, Fan Zhang, Pei Huang, and Jian Zhang. Approximating integer solution counting via space quantification for linear constraints. In *Proc. of IJCAI*, 2019.
- [GMZZ18] Cunjing Ge, Feifei Ma, Peng Zhang, and Jian Zhang. Computing and estimating the volume of the solution space of SMT (LA) constraints. *Theoretical Computer Science*, 2018.
- [GSS21] Carla P Gomes, Ashish Sabharwal, and Bart Selman. Model counting. In *Handbook of satisfiability*. 2021.
- [GT01] Phillip B Gibbons and Srikanta Tirthapura. Estimating simple functions on the union of data streams. In *SPAA*, pages 281–291, 2001.

- [HJ20] Ákos Hajdu and Dejan Jovanović. solc-verify: A modular verifier for solidity smart contracts. In *Proc. of VSTTE*, 2020.
- [KBD⁺17] Guy Katz, Clark Barrett, David L Dill, Kyle Julian, and Mykel J Kochenderfer. Reluplex: An efficient smt solver for verifying deep neural networks. In *Computer Aided Verification: 29th International Conference, CAV 2017, Heidelberg, Germany, July 24-28, 2017, Proceedings, Part I 30*, pages 97–117. Springer, 2017.
- [KDM⁺23] Ipsita Koley, Soumyajit Dey, Debdeep Mukhopadhyay, Sachin Singh, Lavanya Lokesh, and Shantaram Vishwanath Ghotgalkar. CAD Support for Security and Robustness Analysis of Safety-critical Automotive Software. *ACM Transactions on Cyber-Physical Systems*, 2023.
- [KLS97] Ravi Kannan, László Lovász, and Miklós Simonovits. Random walks and an $o^*(n^5)$ volume algorithm for convex bodies. *Random Structures & Algorithms*, 11(1):1–50, 1997.
- [KM18] Seonmo Kim and Stephen McCamant. Bit-vector model counting using statistical estimation. In *Proc. of TACAS*, 2018.
- [KMS⁺18] Samuel Kolb, Martin Mladenov, Scott Sanner, Vaishak Belle, and Kristian Kersting. Efficient symbolic integration for probabilistic inference. In *Proc. of IJCAI*, 2018.
- [KNW10] Daniel M Kane, Jelani Nelson, and David P Woodruff. An optimal algorithm for the distinct elements problem. In *PODS*, pages 41–52, 2010.
- [KS16] Daniel Kroening and Ofer Strichman. *Decision procedures*. 2016.
- [KV97] Ravi Kannan and Santosh Vempala. Sampling lattice points. In *Proc. of STOC*, 1997.
- [LD12] László Lovász and István Deák. Computational results of an $O(n^4)$ volume algorithm. *European journal of operational research*, 216(1):152–161, 2012.
- [Lov91] László Lovász. *How to compute the volume?* DIMACS, Center for Discrete Mathematics and Theoretical Computer Science, 1991.
- [LS90] László Lovász and Miklós Simonovits. The mixing rate of markov chains, an isoperimetric inequality, and computing the volume. In *Proceedings [1990] 31st annual symposium on foundations of computer science*, pages 346–354. IEEE, 1990.
- [LS92] László Lovász and Miklós Simonovits. On the randomized complexity of volume and diameter. In *Proceedings., 33rd Annual Symposium on Foundations of Computer Science*, pages 482–492. IEEE Computer Society, 1992.
- [LS93] László Lovász and Miklós Simonovits. Random walks in a convex body and an improved volume algorithm. *Random structures & algorithms*, 4(4):359–412, 1993.
- [LV06] László Lovász and Santosh Vempala. Simulated annealing in convex bodies and an $o^*(n^4)$ volume algorithm. *Journal of Computer and System Sciences*, 72(2):392–417, 2006.
- [MLZ09] Feifei Ma, Sheng Liu, and Jian Zhang. Volume computation for boolean combination of linear arithmetic constraints. In *Proc. of CADE*, 2009.

- [MMB⁺18] Cristian Mattarei, Makai Mann, Clark Barrett, Ross G Daly, Dillon Huff, and Pat Hanrahan. Cosa: Integrated verification for agile hardware design. In *Proc. of FMCAD*, 2018.
- [MPS17] Paolo Morettin, Andrea Passerini, and Roberto Sebastiani. Efficient weighted model integration via smt-based predicate abstraction. In *Proc. of AAAI*, 2017.
- [MPS19] Paolo Morettin, Andrea Passerini, and Roberto Sebastiani. Advanced smt techniques for weighted model integration. *Artificial Intelligence*, 2019.
- [MVC21] Kuldeep S. Meel, N.V. Vinodchandran, and Sourav Chakraborty. Estimating the size of union of sets in streaming models. In *Proceedings of the 40th ACM SIGMOD-SIGACT-SIGAI Symposium on Principles of Database Systems*, PODS’21, page 126–137, New York, NY, USA, 2021. Association for Computing Machinery.
- [NP23] Aina Niemetz and Mathias Preiner. Bitwuzla. In *Proc. of CAV*, 2023.
- [SM24] Arijit Shaw and Kuldeep S Meel. Model counting in the wild. In *Proc. of Knowledge Representation and Reasoning (KR)*, 2024.
- [Smi84] Robert L Smith. Efficient monte carlo procedures for generating points uniformly distributed over bounded regions. *Operations Research*, 32(6):1296–1308, 1984.
- [SMM⁺22] Giuseppe Spallitta, Gabriele Masina, Paolo Morettin, Andrea Passerini, and Roberto Sebastiani. Smt-based weighted model integration with structure awareness. In *Uncertainty in Artificial Intelligence*, pages 1876–1885. PMLR, 2022.
- [SMM⁺24] Giuseppe Spallitta, Gabriele Masina, Paolo Morettin, Andrea Passerini, and Roberto Sebastiani. Enhancing smt-based weighted model integration by structure awareness. *Artificial Intelligence*, 328:104067, 2024.
- [SSA16] Eric Schkufza, Rahul Sharma, and Alex Aiken. Stochastic program optimization. *Communications of the ACM*, (2), 2016.
- [SSA⁺24] Mate Soos, Uddalok Sarkar, Divesh Aggarwal, Sourav Chakraborty, Kuldeep S Meel, and Maciej Obremski. Engineering an efficient approximate dnf-counter. *arXiv preprint arXiv:2407.19946*, 2024.
- [TW21] Samuel Teuber and Alexander Weigl. Quantifying software reliability via model-counting. In *Proc. of QEST*, 2021.

A Additional Proofs

Claim 1. For $n \in \mathbb{N}$ we have,

$$k^n \leq \frac{1 + \eta/4}{1 - \eta/4}$$

Proof.

$$k^n = \left(\frac{\frac{16n}{\eta} \sqrt{\log \frac{4r}{\eta}} + \kappa}{\frac{16n}{\eta} \sqrt{\log \frac{4r}{\eta}} - \kappa} \right)^n = \left(\frac{\frac{16n}{\eta} \sqrt{\log \frac{4r}{\eta}} + \sqrt{2 \log \frac{4}{\eta}} + \sqrt{2 \log r}}{\frac{16n}{\eta} \sqrt{\log \frac{4r}{\eta}} - \sqrt{2 \log \frac{4}{\eta}} - \sqrt{2 \log r}} \right)^n$$

Now let us focus on the term $\sqrt{2 \log \frac{4}{\eta}} + \sqrt{2 \log r}$. We can bound this term as follows:

$$\begin{aligned} \sqrt{2 \log \frac{4}{\eta}} + \sqrt{2 \log r} &\leq 2 \sqrt{\frac{\log \frac{4}{\eta} + \log r}{2}} && \text{Since } \sqrt{x} + \sqrt{y} \leq 2 \sqrt{\frac{x+y}{2}} \\ &= 2 \sqrt{\log \frac{4r}{\eta}} && \text{Since } \log a + \log b = \log(ab) \end{aligned}$$

Therefore, we can upper bound the term k^n as follows:

$$\begin{aligned} k^n &\leq \left(\frac{\frac{16n}{\eta} \sqrt{\log \frac{4r}{\eta}} + 2 \sqrt{\log \frac{4r}{\eta}}}{\frac{16n}{\eta} \sqrt{\log \frac{4r}{\eta}} - 2 \sqrt{\log \frac{4r}{\eta}}} \right)^n \\ &= \left(\frac{n + \frac{\eta}{8}}{n - \frac{\eta}{8}} \right)^n \\ &= \left(1 + \frac{\frac{\eta}{4}}{n - \frac{\eta}{8}} \right)^n \\ &\leq \exp \left(\frac{n \cdot \frac{\eta}{4}}{n - \frac{\eta}{8}} \right) && \text{Since } 1 + x \leq e^x \text{ for } x \geq 0 \\ &= \exp \left(\frac{\eta}{4} \cdot \left(1 + \frac{\frac{\eta}{8}}{n - \frac{\eta}{8}} \right) \right) \\ &\leq \exp \left(\frac{\eta}{2} \right) && \text{Since for } \eta < n \text{ we have } \frac{\frac{\eta}{8}}{n - \frac{\eta}{8}} \leq 1 \\ &\leq \frac{1 + \eta/4}{1 - \eta/4} && \text{For } \eta < 1 \end{aligned}$$

The last inequality follows from the fact that for $0 < x < 1$, we have $\exp(2x) \leq \frac{1+x}{1-x}$. This completes the proof. \square